Contract No.:

This manuscript has been authored by Battelle Savannah River Alliance (BSRA), LLC under Contract No. 89303321CEM000080 with the U.S. Department of Energy (DOE) Office of Environmental Management (EM).

Alloying of Pu-Al with Stainless Steel for Material Disposition

R. A. Pierce, L. C. Olson, and H. M Ajo, Savannah River National Laboratory, Aiken, South Carolina

Abstract

The Savannah River National Laboratory (SRNL) has evaluated several options for the disposition of stainless-steel clad plutonium metal alloy. One of the technologies under consideration is alloying of the material with stainless steel (SS). The resulting SS-Pu alloy would be a non-proliferable waste form consisting of a secondary Pu composition region microencapsulated in the refractory stainless steel. Two 8-kg ingots were made at SS-1.8Zr-0.4Pu alloys (wt %); 8 kg was determined in a previous study to be the maximum mass of SS ingot at the maximum target Pu loading of 350-g that would result in a SS-4.4Pu alloy (wt %). Two smaller 500-g ingots were also produced at SS-1.6Zr-1.4Pu and SS-1.4Pu (wt %). The 500-g ingots evaluated alloying at a higher Pu concentration than in the 8 kg ingots, and they evaluated the necessity of adding Zr metal to incorporate the Pu and control Pu oxidation. Zr addition was found to be unnecessary to incorporate the Pu and control Pu oxidation. Drill turnings were collected from the large and small ingots and metallographic samples were directly cut from the small ingots. Both were analyzed to validate the structure and composition region formation. Chemical analyses of turnings proved that the Pu was dispersed within the SS ingots.

I. Background

This report addresses research completed for the demonstration of an actinide alloying process to produce Pu waste forms. Metal waste forms (MWF) containing that are metal alloys containing less than 5 wt % Pu are an allowed waste form for disposal of Pu to the Waste Isolation Pilot Plant (WIPP). In these tests, the Pu material was a Pu-10.6 atom% Al alloy (Pu–1.3 wt % Al). The baseline process would generate SS-Pu ingots of about 8-kg with a Pu loading of <5 wt %, which was determined to be the mass for an alloy ingot at the maximum target Pu loading of 350-g.[1] This research included laboratory-scale and prototypic testing using surrogate materials. The laboratory-scale test results were reported in an earlier paper.[1]

The DOE complex has been researching MWFs from U based spent fuels for several decades to sequester actinides in Al, steels, and Zr based alloys. These MWFs are primarily SS with up to 20 wt % Zr and U. The Idaho National Laboratory (INL) MWF phases are dictated by the fuel compositions and enrichments used in the Experimental Breeder Reactor Two (EBR-II) fuel being dispositioned. SRNL has conducted extensive research in dilution of fissile materials and production of non-proliferable MWFs since the late 1990s, including evaluating disposition of U-Al spent fuel in Al melts.[2] Fe-based MWFs were investigated to immobilize metallic radioactive species expected from electrometallurgical treatment methods.[3]

The MWF formulation for the current work has few preconditions because the material under consideration has a relatively pure Pu-10.6Al alloy. According to the Fe-Pu phase diagram, Pu should form an intermetallic Fe_2Pu phase in SS with some limited solid solutioning.[4] Previous research has shown that SS-Zr-Pu and SS-Zr-U alloy microstructures look and behave similar with the same apparent phases.[5,6] Furthermore, SS-Zr-Pu and SS-Zr-U alloys were made with Pu and U concentrations up to 10 wt % and 11 wt %, respectively, that maintained expected microstructures.[5]

The objectives of the present research and development work undertaken were: a) an overall goal to demonstrate ability to microencapsulate SS-clad Pu from a Pu-10.6Al alloy into a stainless steel or Fe-based phase, b) determine if additions of Zr are needed for the alloying chemistry since the previous research included Zr [5,6], and c) compare the efficacy of a preload process with a crane-load process. The furnace and loading equipment were installed in the SRNL shielded cell facility and four tests conducted to produce SS-Pu ingots. Two of the ingots were at the 8-kg size, testing both the pre-loading and crane-

loading of the feed material. Two 500-g ingots were made concurrently in the pre-load configuration to fabricate alloys with and without Zr.

II. Experimental Procedure

II.A Materials

The 304SS used for alloying was obtained through the SRNL Machine Shop. The composition assumed for calculations is 70.24% Fe, 18.0% Cr, 8.5% Ni, 1.2% Mn, 1.7% Si, 0.2% Cu, 0.055% Co, and 0.1% C. The 304SS composition was obtained from a vendor, with the values listed as typical maximum composition and rounded to the nearest tenth of a percent (except for Fe which was calculated from the remaining balance); actual listed elemental values could be off by several percent but is within the 304SS specification. The Zr rod (99.2% purity metals basis) was obtained through Goodfellow (part #356-468-02) and did not have the Hf component removed (Hf >0.2%). The Al foil was Reynolds Foodservice Grade 624 foil with nominal impurities of ~1.5% (Fe+Si). The SS-clad Pu-10.6 alloy came from the SRNL material inventory.

The crucibles for the prototypic-scale and shielded cell tests were purchased from Zircoa. The crucibles in direct contact with the alloys were MgO-stabilized ZrO_2 (MSZ), Alumina crucibles were used to hold the smaller MSZ crucibles used as secondary containment for the 500-g melts. The MSZ crucibles used for the 500-g melts were Zircoa #S-1-3.6 (4.6 cm OD, 3.8 cm ID, 9.1 cm tall). The crucibles used for the 8-kg melts were Zircoa #S-17-9.0 (11.2 cm OD, 9.4 cm ID, 22.9 cm tall). However, the height was reduced at SRNL to make it more consistent for fitting with a head-space purging attachment. An alumina crucible (Zircoa # S-3990-9.0) was used to hold the two 500 g shielded cell melts and was modified in height to fit the same gas purging attachment used for the 8 kg melts. The porosity of the MSZ and for the Al_2O_3 crucibles was 18%.

II.B Test Matrix

Laboratory-scale melts verified alloying behavior and composition development.[1] Several simulant MWF ingots were made to establish and refine operations in the prototypic-size box furnace meant for use in the shielded cells.[1] Following the prototypic-scale furnace validation and testing the test matrix for the shielded cells was reevaluated to maximize resources and likelihood of success. The loaded ingot components are shown in Table 1.

Table 1. Ingot components material masses

Ingot	Alloy type (weight %)	Ingot Total mass (g)	SS (g)	Pu-10.6Al (g)	Zr (g)	[a]Al (g)	Preparation Route
1	SS-1.8Zr-	7460.7	7484.9	27.64	134.5	16.7	Pre-mixed ingredients
2	SS-1.6Zr-	500.4	481.9	6.91	7.9702	3.6	
3	SS-1.4Pu	501.1	490.7	6.91	---	3.8	
4	SS-1.8Zr-	7600.2 [b]	7415.2[b]	27.64	135.0	22.4	Crane loaded Pu

[a]Al present from Al foil used to wrap source components.
[b]The pre-melt mass includes the total mass of the SS basket, which is 136.2 g. It is known that all the basket will not make it into the alloy ingot.

Using the composition for 304SS stated above and the masses of components from Table 1, the calculated atomic concentrations of the elements are listed in Table 2.

II.C Shielded cell furnace fabrication parameters

Minor modifications were made to a CM 17112 BL furnace and operating procedures were established for use in the SRNL shielded cells. The argon cover gas was passed through an inline gas impurity and moisture trap (BMT-4, Agilent Technologies) during the shielded cell operations. For the first two melts, the flow

rate was limited to 5.7 L/min due to a restriction in the gas lines leading to the furnace, but this restriction was reduced for the final melt, and a flow rate of 8.5 L/min was achieved.

Table 2. Ingot calculated atomic % concentrations

Ingot	Cr	Mn	Fe	Ni	Si	C	Pu	Zr	Al
1	20.7	2.0	64.1	9.6	1.5	0.4	0.1	1.1	0.5
2	20.4	1.9	63.4	9.5	1.5	0.4	0.3	1.0	1.5
3	20.6	2.0	64.0	9.6	1.5	0.4	0.3	0.0	1.6
4	20.7	2.0	64.0	9.6	1.5	0.4	0.1	1.1	0.6

The thermal profile for the melts was the same as used for the pre-load simulant melts made during prototypic furnace validation and testing. The furnace thermal profile from the Cycle #2 (making Ingots #2 and 3) and Cycle #3 (making Ingot #4) are shown in Figure 1. For the crane-load test (Ingot #4), the basket was not loaded in until the furnace was at the 1650 °C set-point for approximately 1.5 hr; after the basket loading, the furnace remained at temperature for approximately 1 hr. The furnace profile from Cycle #1 for Ingot #1 (with fuel pre-loaded) was like that for Ingot #4, except it started cooling after being at the 1650 °C set-point for 1.5 hours (compared to 2.2 hours for Ingot #4 [Figure 1]). For the 8-kg ingots, it took the furnace approximately 30 minutes extra to reach the final set-point temperature due to the larger thermal inertia from the alloy.

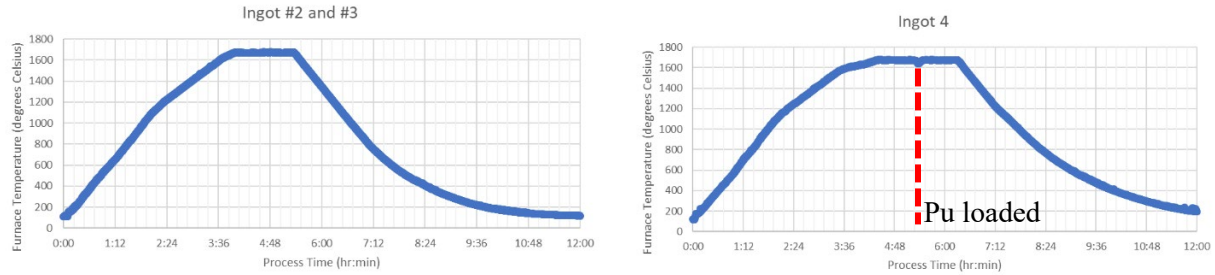

Figure 1. Thermal profiles for Ingots 2 / 3 and Ingot #4. For Ingot 4 the dashed line corresponds to when the Pu charge was loaded, the other ingots were fabricated with the Pu loaded prior to melting.

Ingot sampling was implemented in the shielded cells using drill assembly shown in Figure 2 (Fein, Model# KBM 50Qx 2-1/16 Magnetic Drill). The drill was fixed on top of a clamp apparatus that centered the ingots axially above the drill bit (Figure 2, left). Samples at several different axial locations along the ingot could be taken using the drill and clamp apparatus (Figure 2, right).

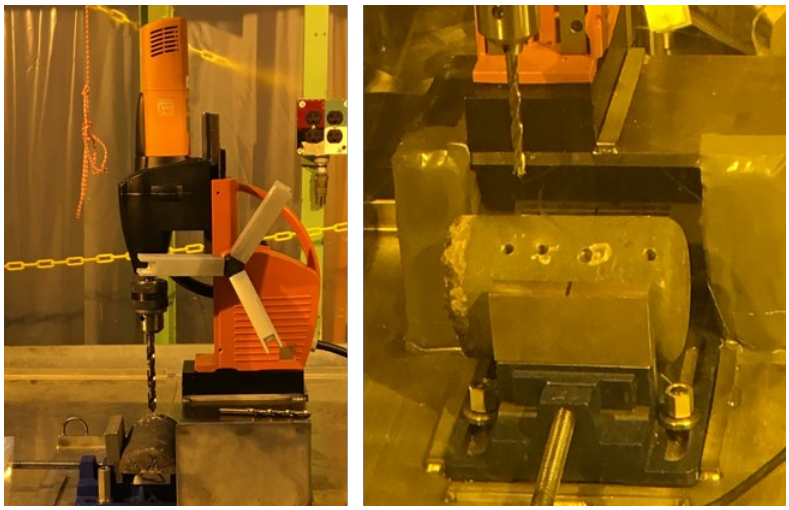

Figure 2. Drill and clamp apparatus (left and sampled ingot (right)

III. Results and Discussion

Several analytical techniques were used, including gravimetric and visual examination, x-ray diffraction (XRD), inductively coupled plasma mass spectroscopy (ICPMS), inductively coupled plasma emission spectroscopy (ICPES), gamma-ray spectroscopy, and scanning electron microscopy / energy dispersive x-ray spectroscopy (SEM/EDS). Controls were implemented in the shielded cells to minimize cross-contamination between the shielded cell environment and the samples.

The analysis of the Pu-bearing ingots focused on 1) proving successful alloying, microencapsulation of the Pu, and 2) micro-capsules containing Pu distribution throughout a large ingot region. The alloys were examined gravimetrically and visually. Drill turnings were taken from four heights for the two 8-kg ingots at a drilled depth varying from approximately 1 cm to 4 cm, and from three heights for the two 500-g ingots at a depth of approximately 1 cm. The drill turnings were partitioned, with some prepared for SEM/EDS, and portions from all sample locations were dissolved for ICPMS, ICPES, and gamma-ray spectroscopy. A piece from a wafer from each of the two 500 g ingots, cut from approximately the horizontal midline, was examined via SEM/EDS to determine microstructural Pu distribution, as opposed to the macrostructural distribution information given by the chemical analyses. After the alloying tests, the crucible caps were analyzed by gamma-ray spectroscopy for deposited radioactive elements.

III.A Gravimetric and Visual Examination

The ingot fabrication occurred like the prototypic-scale furnace validation and testing. There was no cleaning of the ingots. As shown in Table 3, the mass changes were minimal.

Table 3. Ingot masses before and after fabrication

Ingot #	Pre-fab Mass (g)	Post fab Mass (g)	% Mass Change	Notes
1	7460.7	7466.67	0.08	Preload, with Zr, 5.7 L/min argon flow purge
2	500.4	500.32	-0.02	Preload, with Zr, 5.7 L/min argon flow purge
3	501.1	501.75	0.13	Preload, without Zr, 5.7 L/min argon flow purge
4	[a]7600.2	[a]7594.4	[a]-0.08	Top load, with Zr, 8.5 L/min argon flow purge

[a]The full basket mass is included in the before weight, and the post fabrication mass has had 51.5 g added to it, since that was the mass of the basket remnant piece in the prototypic-scale furnace validation and testing crane-load tests.

Post-fabrication images, prior to drill sampling, are shown in Figure 3 for Ingot #1. Ingots #1 and #4 looked similar. The chimney seen in Figure 3 for the cut simulant ingot was apparent in all the simulant ingots, that used ~7.5 kg of 304SS, fabricated in early trials. There were ~10 simulants made during early equipment and process testing, not reported on here for brevity. In contrast to the smaller 500 g ingots which could cool relatively fast and uniformly, the larger masses cooled and solidified first on the edges, forming the chimneys. Because all of the ~7.5 kg simulants that were cut axially showed chimneys, it was assumed the Pu containing ingot would have this feature present as well. Ingots #2 and #3 were not photographed immediately after fabrication. The ingots had some apparent oxide skin on the walls that contacted the crucible, patches of rough oxide skull on the top surface, and a consolidated white patch on the bottom. The consolidated white patch on the bottom is believed to be caused by the bunching of Al foil used to wrap the SS components and accumulation of the BN mold release spray.

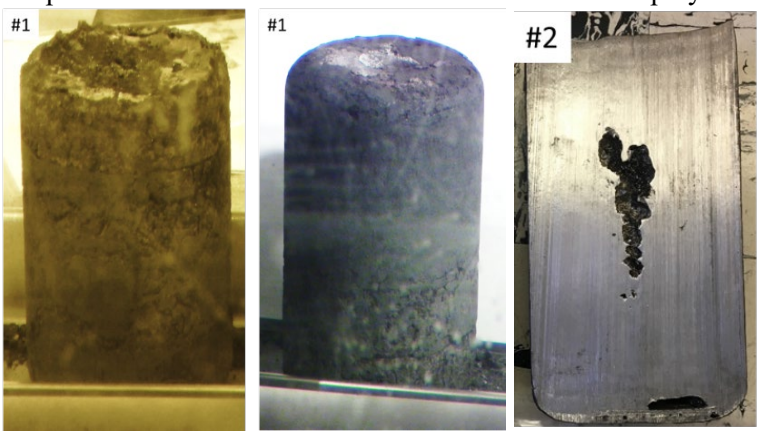

Figure 3. Top of Ingot #1 (left), bottom (center), and cut simulant ingot (right)

III.B Sample Turning Analysis

Samples were extracted from the ingots using a drill shown in Figure 2. Holes in the ingots were drilled with a 3/8-inch (~9.5 mm) drill bit. Although drilling during mock-up activities generated mostly turnings, the samples from the Pu-bearing ingots were mostly chips with a few turnings. The samples were given the designations listed in Table 4.

For the 8-kg ingots, samples were obtained from four locations from the side of the ingot and one from the surface (top mm). For the pre-load 8-kg ingot (#1), the surface sample was taken from the bottom surface; the crane-load 8-kg ingot (#4) surface sample was taken from the top. A picture of the four sample locations from Ingot #4 is provided in Figure 4.

For the 500-g ingots, three samples were collected – one each from the top, middle, and bottom. For SM1, the top and middle samples were taken through the side wall of the ingot while the bottom sample was removed through the bottom face. For SM2, the middle sample was taken through the side wall of the ingot while the top and bottom samples were removed through their respective faces. The SM1 sampling locations are shown in Figure 5.

Table 4. Ingot sampling nomenclature and masses

	Sample ID	Turnings (g)	Sample (g)	Sample Depth** (cm)	Sample Height** (cm)
Ingot #1 7542.77	PL-T1	1.8623	0.3882	2.5 ± 1.5	10 ± 1
	PL-M2*	1.1614	0.3872	2.5 ± 1.5	8 ± 1
	PL-M3*	0.8293	0.2762	2.5 ± 1.5	5 ± 1
	PL-B4	0.9229	0.4802	2.5 ± 1.5	2 ± 1
	PL-S5	0.4945	0.4706	0	0
Ingot #4 7466.67	CL-T1*	1.2077	0.4015	2.5 ± 1.5	10 ± 1
	CL-M2*	0.8126	0.3349	2.5 ± 1.5	8 ± 1
	CL-M3	0.6687	0.4061	2.5 ± 1.5	5 ± 1
	CL-B4	2.1121	0.3902	2.5 ± 1.5	2 ± 1
	CL-S5	2.2833	0.4246	0	13.9 ± 1
Ingot #3 501.75	SM1-T1	1.2917	0.4215	1 ± 0.5	5.6 ± 0.5
	SM1-M2*	1.664	0.4915	1 ± 0.5	2.8 ± 0.5
	SM1-B3	1.9319	0.3842	1 ± 0.5	1.0 ± 0.5
Ingot #2 500.32	SM2-T1	1.3844	0.4391	1 ± 0.5	5.6 ± 0.5
	SM2-M2*	2.0833	0.3986	1 ± 0.5	2.8 ± 0.5
	SM2-B3	1.0343	0.4717	1 ± 0.5	1.0 ± 0.5

* Samples submitted for metallography by CSEM

**Sample Depth is the approximate depth at which turnings were taken for sample analysis, and Sample Height is the axial location on the ingot sample, with the bottom of the sample the 0 point.

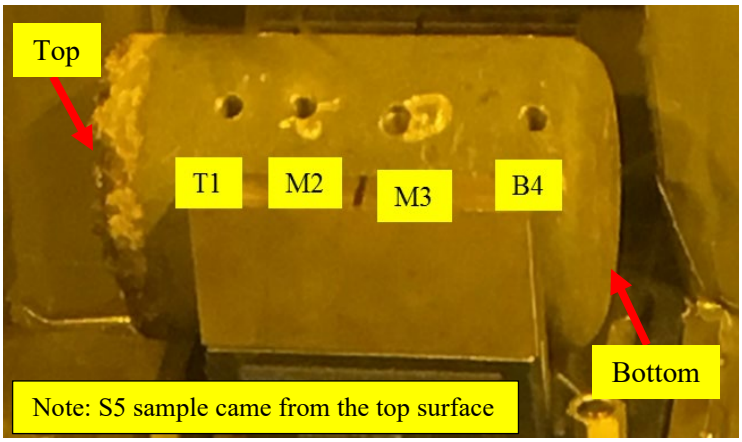

Figure 4. Crane-load ingot (#4) after sampling with sample location designations

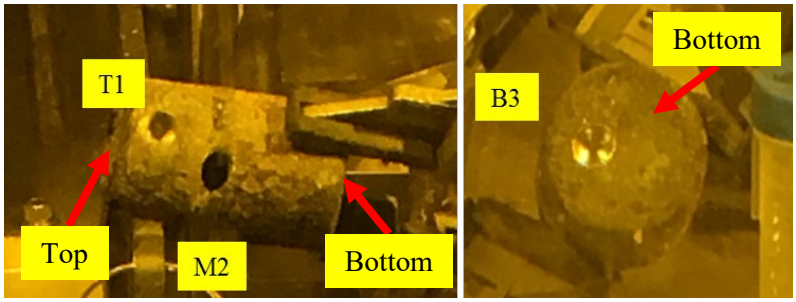

Figure 5. Pre-load ingot (#2, SM1) after sampling with sample location designations

The masses of the ingots prior to drilling, the mass of sample removed by drilling, and the mass of sample turnings submitted to AD are listed in Table 4. The samples were dissolved in 5-mL of hot HNO_3-HCl-HF in a sealed Teflon vessel and then diluted to 50-mL. The dissolved samples were submitted for sequential analyses by ICPMS, gamma-ray spectroscopy, and ICPES. After dissolution of the samples, a residue was noted in Sample PL-S5. The residue was removed by filtration and analyzed by X-ray diffraction (XRD). The XRD spectra showed a mixture of hydrated Pu-fluoride (reported as Np_3F_{12}-H_2O, an analog of PuF_4-H_2O), Pu oxide (PuO_2), and trevorite (Fe_2NiO_4). The quantities of each component in the residue could not be determined. Samples of select turnings were submitted for metallographic analysis by CSEM (Table 4).

III.C ICPMS, ICPES, and Gamma-Ray Spectroscopy

A compilation of the ICPES and ICPMS data which are consistently above the method detection limit is provided in Table 5 for the two 8-kg ingots and Table 6 for the two 500-g ingots. Annotations are included to identify reported results which are significantly different from the expected values. In general, where ICPES and ICPMS analyzed for the same element (Co and Zr), the analyses exhibit agreement.

Table 5. Dissolved turnings data for 8-kg ingots

Element	CL-T1 µg/g	CL-M2 µg/g	CL-M3 µg/g	CL-B4 µg/g	CL-S5 µg/g	CL-Exp µg/g	PL-T1 µg/g	PL-M2 µg/g	PL-M3 µg/g	PL-B4 µg/g	PL-S5 µg/g	PL-Exp µg/g
Al	861	898	796	745	**6040**	2230	1140	1560	2690	1190	**32600**	3000
Co	563	559	551	446	327	540	536	572	534	545	280	540
Co (MS)	572	572	583	549	346	540	549	542	524	541	260	540
Cr	171000	167000	174000	133000	48300	176000	176000	178000	167000	183000	70600	176000
Cu	2010	2000	1960	1590	602	1960	1930	2030	1950	1980	1050	1950
Fe	685000	596000	699000	536000	*305000*	687000	709000	712000	676000	736000	*355000*	686000
Mn	11200	11000	11500	8780	4590	11700	12100	12200	12000	12500	10700	11700
Mo	3270	3280	3200	2550	1120	---	3230	3540	3170	3290	1650	---
Ni	83600	81000	85900	65000	34400	83000	84200	86800	82500	89700	44200	83000
Si	9030	8720	16600	11700	13700	16600	17500	16700	17000	18900	19100	16600
Zr	6700	10400	4260	**26100**	**263000**	17600	6320	7660	19600	12200	**120000**	17800
Zr (MS)	7397	11284	4549	**35048**	**274448**	17600	6456	8059	20433	12344	**124742**	17800
Sum	9.7E+05	8.8E+05	1.0E+06	7.9E+05	6.8E+05		1.0E+06	1.0E+06	9.8E+05	1.1E+06	6.6E+05	

Italicized = low Fe **Bold = high Al and Zr** CL-Exp and PL-Exp are calculated values based on Table 1 masses

Table 6. Dissolved turnings data for 500-g ingots

Element	SM1-T1 µg/g	SM1-M2 µg/g	SM1-B3 µg/g	SM1-Exp µg/g	SM2-T1 µg/g	SM2-M2 µg/g	SM2-B3 µg/g	SM2-Exp µg/g
Al	4880	5260	3110	7380	8070	4150	5190	7770
Co	1390	1390	1060	530	1230	1360	1250	540
Co (MS)	1368	1341	1042	530	1195	1409	1291	540
Cr	174000	164000	159000	174000	155000	167000	166000	176000
Cu	4270	4300	3470	1930	3790	4280	4030	1960
Fe	702000	665000	644000	677000	630000	670000	688000	688000
Mn	12500	11500	10600	11600	11100	11700	11000	11800
Mo	3290	3270	3100	---	3220	3470	3340	---
Ni	82300	76900	75700	82000	72900	78400	78300	83000
Si	16800	12800	10800	16400	12900	22800	19400	16700
Zr	18700	**40800**	23600	15940	**40900**	**23400**	7150	0
Zr (MS)	18858	**43728**	22991	15940	**43253**	286	7353	0
Sum	1.0E+06	9.9E+05	9.3E+05		9.4E+05	9.9E+05	9.8E+05	

Bold = high Zr SM1-Exp and SM2-Exp are calculated values based on Table 1 masses

The data indicate that there are issues with the surface samples (CL-S5 and PL-S5) of the 8-kg ingots. In both ingots, the Fe is low, the Al is high, the Zr is extremely high, and the material balance 30-35% low. The large Al concentrations could be explained by the Al used to wrap the alloying components before heating or from the wrapped components in the Al packed basket during the crane-load operation. The sample taken from the bottom surface from the preload was from a region where the Al foil was bunched up and folded in on itself. The sample from the top of the crane-load could have had the Al foil from the crane-load basket mostly stay on the surface. In the crane-load basket, Al foil was used to wrap the Zr rods, SS-clad Pu-10.6Al, and pack the basket to keep these from moving during transport. During introduction of the basket into the furnace, the Al foil (Al mp = 660 °C) would melt immediately during introduction and probably drip out of the basket to remain on the surface, where it could oxidize during the basket introduction step (argon cover was temporarily stopped during this step).

The high Zr level could have been from zirconia that fell in from the lid onto the surface for the crane-load surface sample, or that was peeled off from the crucible bottom for the pre-load sample, other loose pieces of zirconia from the crucible or lids that made it to the sample locations, or from the Zr metal components that migrated to the surface locations. For the crane-load ingot, as the basket was pushed into the melt, it is unknown exactly how the loaded components distributed and melted. It is possible some of the Zr rods were pushed out of the basket by a thick SS melt. The presence of very high Zr could impact the presence of Fe and the ability of AD to dissolve the Zr (with fluoride) to obtain a good mass balance. Zr is an effective complexant for aqueous fluoride ions.[7] If the basket and all or most of components loaded in it stayed in during the plunge into the molten ingot, then those components could have made it within ~2 cm to 4 cm from the bottom of the ingot, and perhaps this explains the presence of high Zr in the CL-B4 turning sample. However, it is also possible the Zr in this turning sample originated from the crucible. The presence of high Zr could have impacted the ability of AD to completely dissolve the sample.

The high Zr values for the 500-g ingots require significant consideration. For Test SM1, the data show distribution of Zr to the top (SM1-T1) and bottom (SM1-B3) samples, although the highest concentration is in the middle (SM1-M2). This is not surprising because the Zr was initially loaded at the center of the pre-loaded ingot. More difficulties are encountered for Test SM2 when trying to understand the high Zr values in the top because the pre-loaded ingot did not include any Zr. The low concentration of Zr in the bottom sample (SM2-B3) could be the result of interaction between crucible and the ingot (the sample was drilled from the bottom, and a sheath of crucible appears to stick to the ingot). The high concentration of Zr in the top sample (SM2-T1) could be the result of crucible and lid degradation (the sample was drilled from the top rather than the side, as was the case with SM1-T1), but that case is more difficult to make because the top of the ingot is not in contact with the crucible lid and the likelihood of degradation products coming from the lid is low. The mass balances for all 500-g ingots were within the 10% method uncertainty for ICPES.

Table 7 provides a comparison of the gamma-ray spectroscopy and ICPMS data. Although the gamma-ray spectroscopy and ICPMS data do not show uniform distribution of Pu in the ingots, they do confirm that Pu has distributed in all four ingots. There are not distinct areas of Pu metal that can be readily separated from the ingot. Although not uniform, the gamma-ray spectroscopy data for Pu indicates a good mass balance. The mass balance for the 8-kg pre-load sample is a little low, but it does not include the Pu identified in the residue of dissolved PL-S5 turnings. It can be questioned whether taking an average of the analyses provides an accurate assessment of the mass balance, especially considering the issues associated with CL-S5 and PL-S5. However, absent either larger or a greater number of samples, the data provide a good approximation of accounting for all Pu.

Table 7. Comparison of gamma-ray spectroscopy and ICPMS Pu data for dissolved turnings

Sample	Gamma Tot Pu wt %	Gamma Avg Pu wt %	ICPMS Tot Pu wt %	ICPMS Avg Pu wt %	Target Tot Pu wt %	ICPMS vs Gamma % Diff.
CL-T1	0.187		0.197			-5.4
CL-M2	0.133		0.146			-9.8
CL-M3	0.152		0.155			-2.4
CL-B4	0.231		0.229			0.8
CL-S5	0.967	0.334	0.760	0.298	0.36	21.4
PL-T1	0.180		0.141			21.7
PL-M2	0.196		0.170			13.2
PL-M3	0.537		0.358			33.4
PL-B4	0.233		0.187			19.4
PL-S5*	**0.398**	**0.309**	**0.273**	**0.226**	0.36	31.4
SM1-T1	0.943		0.662			29.8
SM1-M2	2.438		1.245			48.9
SM1-B3	0.863	1.415	0.618	0.842	1.35	28.4
SM2-T1	1.423		1.180			17.1
SM2-M2	2.118		0.766			63.9
SM2-B3	0.344	1.295	0.279	0.742	1.35	18.8
*** Does not account for Pu in PL-S5 residue**						

The discrepancy between ICPMS and gamma data is a concern, as indicated in the last column of Table 7 which compares the difference between the ICPMS and gamma values. The calculations are based on the gamma data because gamma spectroscopy is a reference method at SRNL for Pu accountability; ICPMS is not used for accountability because of its stated uncertainty of 20% versus a typical uncertainty for Pu-239 of 5.0%. Much of the data for the two methods fall within the combined uncertainty of the two methods, but several values are outside of the combined uncertainty. The reason for the discrepancy is unknown because samples for gamma and ICPMS were drawn from the same solution of dissolved ingot.

The distribution of Pu in Test SM2 is significant. It was the only test performed without the addition of Zr metal. Zr was added to aid suppression of PuO_2 formation, which facilitates alloy formation with the Pu. The results of Test SM2 indicate that the addition of Zr was not necessary for alloy formation. The omission of Zr from the alloy should enable the use of high-density alumina crucibles instead of what was used in these tests – low-density magnesia-stabilized zirconia. The high-density alumina crucibles are less expensive, react less with the alloy, and provide a better barrier to air diffusion through the crucible wall onto the surface of the alloy.

Better distribution of the Pu in the system could be accomplished through a system with better atmosphere control, especially using a pre-load configuration. It would also help to use high-density alumina crucibles instead of low-density zirconia crucibles. It is likely that slightly higher alloying temperatures and longer dwell times would provide more-uniform ingots.

The gamma-ray spectroscopy data for Pu agree with the ICPMS for the first four samples. It was confirmed that the ICPMS samples were analyzed in the order displayed in Table 7. The divergence of the ICPMS data from the gamma-ray spectroscopy data points to an issue with the ICPMS data because all subsequent ICPMS data are lower than the corresponding gamma-ray spectroscopy data.

In general, the data of Table 5 and Table 6 show that Am-241 concentration corresponds to that of Pu at a ratio of about 130 to 150 Pu:Am-241. This suggests that the Am-241 is not preferentially volatile, but rather retained within the alloy structure. There appears to be no correlation between the location of Pu and that of Cs-137.

III.D SEM/EDS Ingots #1 and #4

In the following discussion, the EDS results were evaluated both with and without oxygen. It is possible a large portion of the EDS oxygen signal is from an oxide formed on reactive metal surfaces after polishing. For the sake of brevity, and because of the potential oxygen contamination, only the data without oxygen are reported. For the EDS analysis, in general, several EDS point scans were taken of each apparent characteristic region. Usually, three EDS point scans for each characteristic region at a minimum were attempted to be taken, so that an average and standard deviation in the measurement could be reported. The apparent characteristic regions were determined visually, i.e., matrix, locations darker than the bulk, brighter than the bulk, intermediate brightness than the bulk, etc.

Drill turnings were taken from similar regions of both 8 kg alloys, with the crane loaded (CL) alloy in Figure 4 showing the locations of the samples and origin of the second part of the ~8 kg sample names in Table 8.

Table 8. SS-Pu alloys samples

Sample	Fabrication	Ingot Size	Alloy (wt%)	Sample Type
CL-T1	Crane load	8 kg	SS-1.8Zr-0.4Pu	Drill turning
CL-M2	Crane load	8 kg	SS-1.8Zr-0.4Pu	Drill turning
PL-M2	Pre-load	8 kg	SS-1.8Zr-0.4Pu	Drill turning
SM1	Pre-load	500 g	SS-1.6Zr-1.4Pu	Wafer cut from center
SM2	Pre-load	500 g	SS-1.4Pu	Wafer cut from center

Sample CL-T1 was from a drill turning from the top of the crane loaded ingot, with drill turnings collected ~1 cm below the surface. All the drill turning samples are assumed to have undergone cold work and perhaps heating from the drilling sample method that could change the structure of the cast compositions. The change in structure of the Pu-rich compositions from cold working is not expected to affect the analysis of the Pu distribution or microencapsulation. For the crane loaded ingot, the basket holding the Pu and Zr charge should have pushed the Pu and Zr down near the bottom of the ingot, provided the elements stayed located within the basket during the travel through the ~1650 °C molten 304SS. However, Figure 6 shows bright compositions within the 304SS that are indicative of Pu or Zr rich composition regions, indicating the Pu was well dispersed in the sample and not only at the bottom.

Figure 6 shows the locations of the EDS point scans, and the concentrations are normalized without oxygen in Table 9. Pu rich and Zr rich regions were observed. The likely ferrite and austenite phases were not observed in the samples made from drill turnings, either obscured by scratches form inadequate polishing or from morphology changes brought on by coldwork from the sampling method.

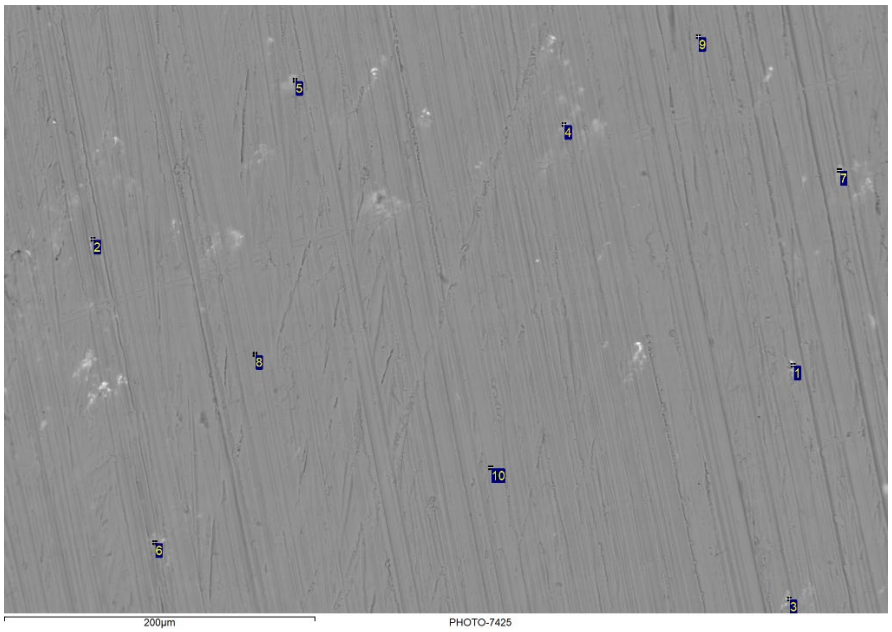

Figure 6. Regions of EDS point scans on sample CL-T1. White regions are Pu or Zr rich. Diagonal lines caused by inadequate polishing.

Table 9. EDS point scans, without oxygen, corresponding to Figure 6 (CL-T1). Results in at%.

Spectrum	Si	S	Cr	Mn	Fe	Ni	Zr	Pu	Group
1,3,4	---	2.4-5.0	18.2-19.0	1.2-1.3	58.4-60.9	6.2-7.2	1.7-7.3	5.4-8.1	Pu rich
5,6,7	---	---	10.4-17.0	0-1.2	31.9-53.4	3.7-7.6	20.9-53.2	0-0.8	Zr rich
8,9,10	0.8-1.5	---	19.9-20.4	1.3-1.4	69.1-69.8	7.8-8.1	---	---	bulk matrix

Sample CL-M2 was a drill turning above the midline of the crane loaded ingot (see Figure 4). SEM images of this sample differ little from that of CL-T1 discussed above (Figure 6) and, therefore, are not included. As with CL-T1, it is evident brighter regions characteristic of Pu and Zr rich compositions are present in CL-M2, further validating that the Pu is distributed throughout the ingot. The EDS point scan results for CL-M2 are tabulated in Table 10 without oxygen. Three classes of compositions were evident, one rich in Pu, one rich in Zr, and the bulk 304SS matrix.

Table 10. EDS point scans, without oxygen, for CL-M2. Results in at%.

Spectra	Si	P	S	Cr	Mn	Fe	Ni	Zr	Pu	Group
1,2,3	---	0-23.1	0-7.8	9.1-21.7	---	28.0-57.0	4.3-19.4	0-10.1	7.2-20.3	Pu rich
4,6,10	---	---	0-1.3	11.6-18.2	0.8-1.3	36.2-57.5	4.1-6.6	11.9-47.4	0-3.5	Zr rich
7,8,9	1.1-1.5	----	---	20.0-21.0	1.1-1.4	69.1-69.7	7.3-8.0	---	---	bulk matrix

Sample PL-M2 was a drill turning above the midline of the preloaded ingot (Figure 4). This ingot was preloaded with Pu and Zr, with those components being held in a loosely sealed cup near the center of the 304SS components. Of the loading methods evaluated during simulant tests, this loading strategy is believed to allow for the least amount of interaction of the Pu and Zr with the crucible walls and oxygen contamination.

Figure 7 shows an image of the polished turning sample, and it is evident brighter regions characteristic of Pu and Zr rich compositions are present. There appears to be more of the bright compositions than in the CL turnings. The analyses of the EDS point scans in Figure 7 are tabulated in Table 11 without oxygen. Once again, three classes of compositions were evident, one rich in Pu (white), one rich in Zr (light gray), and the bulk 304SS matrix (dark gray).

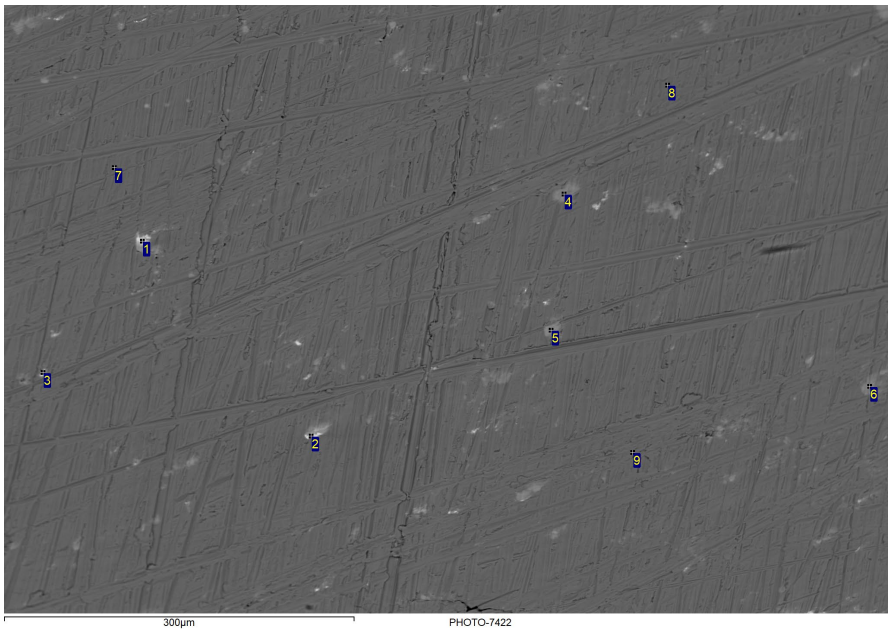

Figure 7. PL-M2 sample showing locations of EDS point scans. White regions are Pu or Zr rich. Diagonal and cross-hatched lines caused by inadequate polishing.

Table 11. EDS point scans, without oxygen, corresponding to Figure 7 (PL-M2). Results in at%.

Spectra	Si	Cr	Mn	Fe	Ni	Zr	Pu	Group
1,2,3	---	7.3-11.3	1.2-1.5	32.9-38.8	29.4-32.2	2.2-9.1	14.8-19.6	Pu rich
4,5,6	2.3-4.2	9.9-11.1	0.7-0.9	50.2-52.5	12.2-13.5	19.4-22.4	0-0.4	Zr rich
7,8,9	0-1.0	20.1-20.9	1.3-1.5	69.3-70.3	7.2-8.2	---	---	bulk matrix

The SEM and EDS analyses results of Ingots #1 and #4 appear to show successful alloying and microencapsulation of the Pu, and good microencapsulant distribution throughout a large ingot region.

III.E SEM/EDS Ingots #2 and #3

In the following discussion, the EDS results were evaluated both with and without oxygen. It is possible a large portion of the EDS oxygen signal is from an oxide formed on reactive metal surfaces after polishing. For the sake of brevity, and because of the potential oxygen contamination, only the data without oxygen

are reported. For the EDS analysis, EDS point scan locations and numbers were chosen as described previously for Ingots #1 and #4.

The two smaller ingots had a wafer cut from the middle region using a water-cooled slow speed diamond saw, and a section of this wafer was cut out for analysis (Figure 8). These samples were mounted in EpoFix, then ground and polished for SEM/EDS. The wafer cut pieces are believed to better represent the microstructure of potential SS-Pu alloys since the drill turnings are more likely to have been affected by coldwork and heat during the dry drilling process.

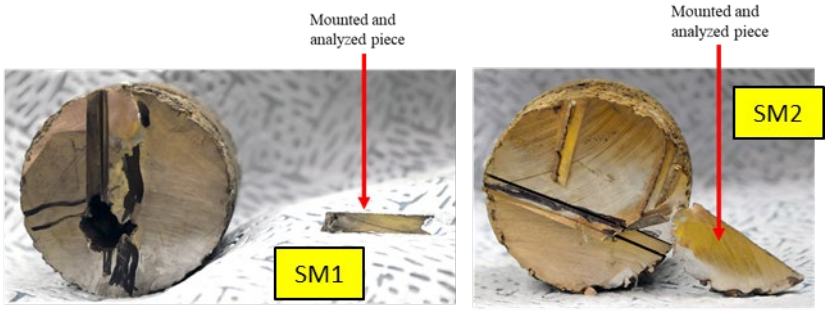

Figure 8. Small ingots SM1 and SM2 showing location of sample for SEM/EDS

Ingot SM1 was fabricated to be SS-1.6Zr-1.4Pu wt%. Back scatter detector (BSD) images were collected from the ingot SM1 sample shown in Figure 8. The images show good distribution of brighter (Pu-rich) throughout. A comparison of a BSD image, in which heavier elements appear brighter, and its corresponding secondary electron (SE) detector image, which shows topology better, indicates that the Pu composition in the images is part of the alloy, and not merely a surface contaminant. It also shows that the dark regions in the BSE image are enriched in lower atomic weight elements compared to the rest of the 304SS matrix rather than being pits in the surface.

Figure 9 shows the locations of EDS point and area scans with the corresponding results in Table 12 (oxygen excluded). Four general compositions are identified in Table 12. There are Pu-rich compositions, Zr-rich compositions, darker compositions believed to correspond to Cr rich and Ni poor ferrite, and Cr poor and Ni rich austenite. EDS spectrums 22 and 23 correspond to large area EDS scans. Spectrum 23 partially covers 22 with acquisition times of 90 and 300 seconds, respectively.

The data from Table 12 show that the light particles in the SEM images are Zr and Pu rich. In the alloy bulk, the dark regions of the BSD images corresponding to ferrite were found to be Cr rich and Fe poor, and the brighter regions corresponding to austenite are Cr poor and Ni rich. Cr is a ferrite stabilizer, and Ni an austenite stabilizer. The large area raster scans averaged out the austenite and ferrite regions. Pu and Zr have larger metallic radii than the austinite and ferrite components, Fe, Ni, and Cr, and were expected to be rejected from the bulk matrix into interdendritic regions upon cooling. Of note, is that the bulk alloy EDS point and large area raster scans did not show evidence of any Pu or Zr, so the Pu in the alloy was successfully microencapsulated by forming a Pu-Zr rich composition.

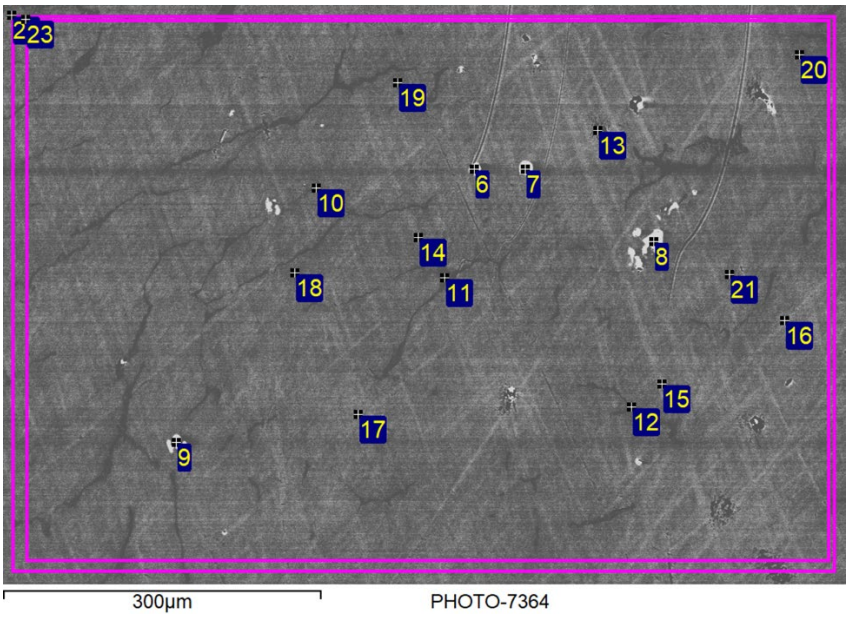

Figure 9. BSD image of SM1, with EDS point scan locations 6 through 23 marked. White regions are Pu or Zr rich. Diagonal lines caused by inadequate polishing. Dark regions are Cr rich.

Table 12. EDS point scans, without oxygen, corresponding to Figure 9 (SM1). Results in at%.

Spectra	Si	Cr	Mn	Fe	Ni	Zr	Pu	Group
7,9	---	2.8-3.8	0-4.6	6.6-9.5	---	37.5-39.4	47.2-48.5	Pu rich
6,8	---	1.2-1.4	---	3.0-3.2	---	89.2-94.2	1.6-6.2	Zr rich
10,11,12	1.0	27.1-27.8	1.1-1.3	67.2-67.8	2.9-3.2	0.0	0.0	ferrite
14-21	0.9-1.1	19.7-20.9	1.3-1.5	69.8-70.4	6.6-8.0	0.0	0.0	austenite
22	0.9	20.7	1.4	69.8	7.2	0.0	0.0	large area scan
23	0.9	20.6	1.5	69.8	7.2	0.0	0.0	

Figure 10 shows a BSD image at higher magnification of the Pu rich particles. EDS analysis (Table 13) show that some of the Pu rich particles have high Zr concentrations and may be oxides. The particles also had significant sulfur concentrations, with more sulfur being present for higher Pu concentrations, indicating the possible formation of a new plutonium sulfide phase not observed in the uranium surrogate. While multiple sulfides have been reported in the literature [8], there are none that have been reported that have higher ratio of Pu to S that could entirely account for the S. It is possible that the S corresponds to a Fe, Cr, or more complex mixed S phase. It is not known where the sulfur originated, but it does not appear to impede the microencapsulation of the Pu. It is possible the sulfur is a surface contaminant or an error in the EDS peak matching software package used by the SEM.

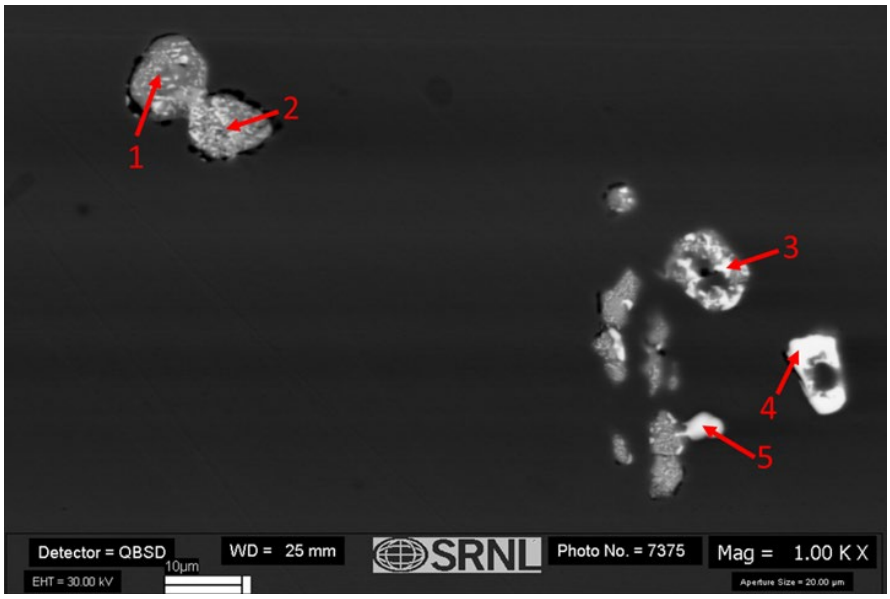

Figure 10. SM1 cross-section view showing EDS point scans of Zr-Pu rich particles. Brighter regions are Pu and Zr rich, with Pu being especially bright. Dark regions are Cr rich.

Table 13. EDS point scans, without oxygen, corresponding to Figure 10 (SM1). Results in at%.

Spectra	Al	S	Cr	Mn	Fe	Ni	Zr	Pu
1	4.2	7.3	1.5	0.0	3.8	0.0	66.8	16.5
2	6.9	10.7	2.0	0.9	3.6	0.0	60.2	15.7
3	0.0	24.3	4.8	0.0	12.1	0.0	18.9	39.9
4	0.0	28.8	3.6	0.0	9.4	0.0	3.2	55.1
5	0.0	15.0	14.3	1.1	42.0	4.1	0.0	23.6

Ingot SM2 was fabricated to be SS-1.4Pu wt%. Back scatter detector (BSD) images were collected from the ingot SM1 sample shown in Figure 11 and Figure 12. The EDS results are tabulated without oxygen in Table 14 and Table 15, respectively. Although SM2 was fabricated without Zr metal, some Zr was detected within the Pu rich compositions. It is hypothesized the Zr could have been partially reduced from the crucible or transferred to the surface of the sample as contamination during sample grinding/polishing.

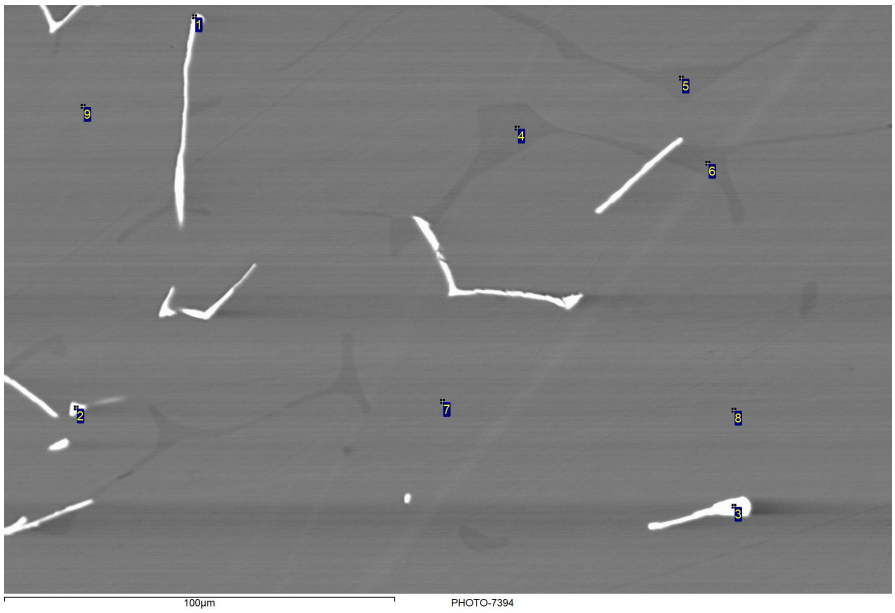

Figure 11. BSD image near center of ingot SM2. Brighter regions are Pu and Zr rich. Dark regions are Cr rich.

Table 14. EDS point scans, without oxygen, corresponding to Figure 11 (SM2). Results in at%.

Spectra	Al	Si	S	Cr	Mn	Fe	Ni	Zr	Pu	Group
1,2,3	---	---	---	10.1-18.4	---	26.5-50.2	2.1-4.1	2.7-8.2	24.6-53.1	Pu rich
4,5,6	0-0.9	0.9-1.0	0-0.4	26.6-27.0	1.0-1.1	67.3-68.0	2.8-2.9	---	---	ferrite
7,8,9	---	0-0.9	---	19.6-19.8	1.3	70.9-71.5	7.3-7.7	---	---	austenite

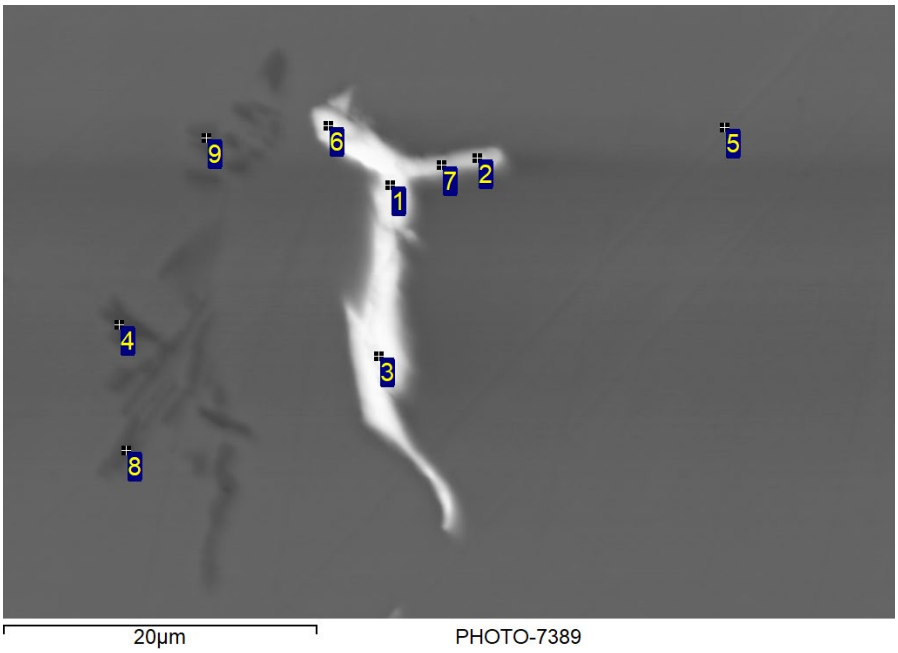

Figure 12. High magnification BSD image from SM2 showing Pu rich (light region) and Cr rich (dark regions) precipitates.

Table 15. EDS point scans, without oxygen, corresponding to Figure 12 (SM2). Results in at%.

Spectra	Si	S	Cr	Mn	Fe	Ni	Zr	Pu	Group
1,3,6	0-3.9	---	8.1-10.9	---	21.2-23.4	2.0-2.4	6.2-6.6	53.5-60.8	Pu rich
2,7	1.8-2.4	---	18.2-19.0	0-1.3	47.7-48.6	5.1-5.3	2.6-2.8	22.1-23.2	Pu rich
4,8,9	---	0-0.5	37.6-50.1	1.4	46.4-55.6	2.1-4.5	---	---	Cr rich
5	0.9		21.0	1.6	67.0	8.8			bulk matrix

The SEM and EDS analyses results of Ingots #2 and #3 appear to show successful alloying and microencapsulation of the Pu, and good microencapsulant distribution throughout a large ingot region.

IV. Conclusions

SRNL demonstrated in its shielded cells facility the capability to alloy SS-clad Pu-10.6Al at% alloy with SS to form a SS-Pu alloy. Full-scale 8-kg ingots were fabricated at 0.4 at% Pu and 500-g ingots were fabricated at 1.4 at% Pu. One 8-kg ingot was made with a pre-load configuration and another 8-kg ingot with a crane-load configuration. It is recommended to use pre-loading of component materials to simplify design and reduce possible avenues for air ingress.

Samples taken from the ingots for chemical and metallurgical analyses demonstrate the distribution of the Pu in all four ingots. Evidence points to Zr not being necessary to distribute the Pu within the alloy. The ingot without Zr appeared to have a sufficient Pu distribution. Analogy with SS-15 weight % Zr-Pu ingots indicates the Pu should be distributed in a microencapsulated composition region, although further SEM/EDS work is needed to confirm this. The ability to operate without Zr could greatly improve melt

quality by allowing for the use of alternative crucible materials such as high-density alumina. Further development is recommended to demonstrate better atmosphere controls.

Oxidation of the melts during fabrication was observed, and interaction between the melts and the highly porous and low-grade purity crucible occurred. The analysis of turnings drilled from the ingots appears to be sufficient for general mass accounting. Based on the turning analysis, the preload and crane-loaded ingots presented similar Pu distributions.

For all the samples investigated by SEM and EDS, Pu rich compositions were present and well distributed. The diamond saw cut samples had better observable microstructure compared to the drilled samples due to less coldworking. Ferrite, austenite, Pu rich, and Zr rich compositions were detected in the samples. Some of the Pu rich compositions were as high as 61 at% Pu. The presence of potential Pu-S bearing compositions was noted in some alloys. In all cases, the Pu rich compositions in the bulk alloys appeared to be encapsulated by stainless steel.

V. References

1. Olson, L., Pierce, R., Actinide Alloying Studies, SRNL-TR-2018-00139, May 2018.
2. Vinson, D., Adams, T., Duncan, A., Lee, S., Characteristics of the Melt-Dilute Form of Aluminum-Based Spent Nuclear Fuel, in Savannah River Technology Center technical document, WSRC-TR-2002-00128. 2002.
3. McDeavitt, S., Abraham, D., Park, J., Evaluation of stainless steel-zirconium alloys as high-level nuclear waste forms. Journal of Nuclear Materials, 1998. 257: p. 21-34.
4. Baker, H., ASM Handbook: Alloy Phase Diagrams, Volume 3, 1992.
5. Keiser, D., Abraham, D., Sinkler, W., Richardson, J., McDeavitt, S., Actinide distribution in a stainless steel±15 wt% zirconium high-level nuclear waste form. Journal of Nuclear Materials, 2000. 279: p. 234-244.
6. Janney, D.E., Host phases for actinides in simulated metallic waste forms. Journal of Nuclear Materials, 2003. 323: p. 81–92.
7. Tallent, O.K., Mailen, J. C., Effects of metal ion impurities on PuO2 dissolution in nitric-hydrofluoric acid solution. Nuclear Technology, 1977. 34.
8. F. H. M. Ellinger, W.N.; O'Boyle, D.R. & Schonfeld, F.W., "Constitution of Plutonium Alloys," p. 95, Los Alamos Technical Report, LA-3970, January 1 1968.